Proceedings of HT2007
2007 ASME-JSME Thermal Engineering Summer Heat Transfer Conference
July 8-12, 2007, Vancouver, British Columbia, CANADA

HT2007-32046

TOPICS OF HEAT TRANSFER RELATED TO SINGLE-WALLED CARBON NANOTUBES

Shigeo Maruyama
Department of Mechanical Engineering
The University of Tokyo
7-3-1 Hongo, Bunkyo-ku,
Tokyo, 113-8656, Japan

ABSTRACT

Using an alcohol catalytic CVD method shown to produce high-quality single-walled carbon nanotubes (SWNTs), films of vertically aligned (VA-)SWNTs were synthesized on quartz substrates. The VA-SWNTs can be removed from the substrate and transferred onto an arbitrary surface—without disturbing the vertical alignment—using a hot-water assisted technique. This ability makes experimental measurements of the anisotropic properties of SWNTs considerably less challenging.

A series of molecular dynamics simulations have been performed to investigate a variety of heat conduction characteristics of SWNTs. Investigations of stationary heat conduction identifies diffusive-ballistic heat conduction regime in a wide range of nanotube-lengths. Furthermore, studies on non-stationary heat conduction show that the extensive ballistic phonon transport gives rise to wave-like non-Fourier heat conduction. Finally, several case studies are presented for SWNT heat transfer in more practical situations.

INTRODUCTION

Single-walled carbon nanotubes (SWNTs) are rolled-up tubes of single-layer graphite, which have a diameter on the order of 1 nm. They have been shown to have remarkable electrical, optical, mechanical and thermal properties [1], making them not only interesting from a purely scientific perspective, but also highly desirable for development of many new applications. As a result, SWNTs have been the focus of numerous investigations in numerous fields of science and engineering. However, one challenge facing many of these studies is control over the morphology of synthesized SWNTs. A significant development in morphology control came when the alcohol catalytic CVD technique [2] was combined with a simple dip-coat preparation of catalytic metal particles. The result was vertically aligned (VA-)SWNT films [3, 4] synthesized on quartz substrates. These films can exceed 30 μm in thickness, and consist of thin, vertically aligned SWNT bundles [5]. Their use in various applications is becoming more and more promising, and VA-SWNT synthesis has recently been achieved by several other groups [6-12]. In the heat transfer community, the expected high thermal conductivity of SWNTs [13] has attracted a number of studies over the past few years. Recent activities in our group directed at experimentally measuring the thermal conductivity of our aligned SWNT films will be discussed.

With advances in SWNT synthesis and MEMS techniques, thermal conductivity (or thermal conductance) measurements of individual SWNTs have been recently reported [14, 15]. However, the thermal property measurements of SWNTs in experiments are extremely challenging as there are potential uncertainties residing in the technicality related to, for instance, the contact resistances between thermal reservoirs and an SWNT. Therefore, the demands for reliable theories and numerical simulations are greater than ever for validation of experimental results and for detailed investigation of heat-conduction characteristics that are not accessible in experiments. Molecular dynamics (MD) simulations have been a strong tool for the investigation of thermal conductivity of SWNTs. The diffusive-ballistic phonon transport regime covers a wide range of nanotube-lengths in actual applications due to the extraordinary long phonon mean free path at room temperature. This gives rise to various unique stationary and non-stationary heat conduction characteristics.

A unique aspect of the heat conduction of an SWNT can be seen in the length dependence of the thermal conductivity. For SWNTs, due to the expected long phonon mean free path, the regime of the length effect stretches beyond the realistic length in many applications. The length effect has been demonstrated using MD simulations [16, 17] and the power-law divergence was discussed with analogy to conventional one-dimensional

models [18]. More recently, the length effect was investigated up to the fully diffusive phonon transport regime using a kinetic approach [19], where the divergence was shown to disappear with presence of second (or higher) order 3-phonon scattering processes. In the current study, the length effect is investigated by performing MD simulations for a wide range of nanotube-lengths in excess of one micrometer.

Non-stationary heat conduction of SWNTs has been investigated by non-stationary MD simulations, where a heat pulse is generated as coherent fluctuations by connecting the local cell to the thermostat for sub-picosecond duration [20]. As the excitation is done in terms of collective phonons, the simulation allows us to investigate the possibility of non-Fourier heat conduction [21, 22]. The excitation and the evolution can be decomposed to temporal evolution of spectral bands by performing wavelet transformations, which allow us to observe diffusive and ballistic features of the phonon transport.

Furthermore, several more issues of heat transfer in practical situations can be investigated using MD simulations. Attenuation of the expected high thermal conductivity was simulated by mixing ^{13}C isotope impurities within SWNTs, or by binding two SWNTs of different chirality with a junction structure between them [23, 24]. The heat transfer through the junction can be expressed with the thermal boundary conductance by considering a virtual boundary at the junction.

SYNTHESIS OF VERTICALLY ALIGNED SWNTS

There are many methods of single-walled carbon nanotube (SWNT) production, each with different merits and demerits, but methods related to chemical vapor deposition (CVD) are widely considered the most promising. The synthesis of SWNTs is notoriously more difficult than multi-walled carbon nanotubes. This is primarily related to the difficulty in preparing catalyst particles of the appropriate size (1-2 nm in diameter), and preventing these particles from agglomerating at the elevated growth temperature. The reaction of the carbon feedstock gas is also a critical factor determining the type and quality of nanotubes produced.

The first reported synthesis of vertically aligned (VA-) SWNTs stemmed from the discovery of the alcohol catalytic CVD method [2]. It was found that using alcohol as the carbon source preferentially synthesized high-purity, high-quality SWNTs (figure 1). The catalyst particles used to grow these SWNTs were zeolite-supported Fe and Co particles, which were infused into the zeolite by sonication in an ethanol solution [2(and references therein)]. This catalyst preparation procedure was modified to deposit mono-dispersed catalyst particles onto a flat substrate surface. Compared with the zeolite method, replacing Fe with Mo was found to significantly increase the overall yield, and with the right concentration of each metal species (0.01 wt%), the resulting SWNTs grew vertically aligned [3], as shown in figure 2.

The substrate—usually quartz—is immersed into a solution containing dissolved metal acetates. After soaking for several minutes, the substrate is slowly withdrawn at a constant speed of 4 cm/min. After withdrawing the substrate from the dip-coat solution, it is baked in air at 400 °C for 5 minutes to oxidize the metal particles. The dip-coat method coats the substrate with a thin, uniform liquid layer of the homogeneous mixture, which results in dense, mono-dispersed catalyst particles on the substrate surface. Immediately prior to CVD growth of SWNTs, the sample is placed in an electric furnace, where it is heated under 40 kPa of flowing Ar/H_2 (3% H_2) up to the synthesis temperature of 700-800 °C. The presence of H_2 during this stage reduces the oxidized particles, making them catalytically active. Once reaching the synthesis temperature, the Ar/H_2 flow is stopped, and ethanol vapor is introduced for typically 10

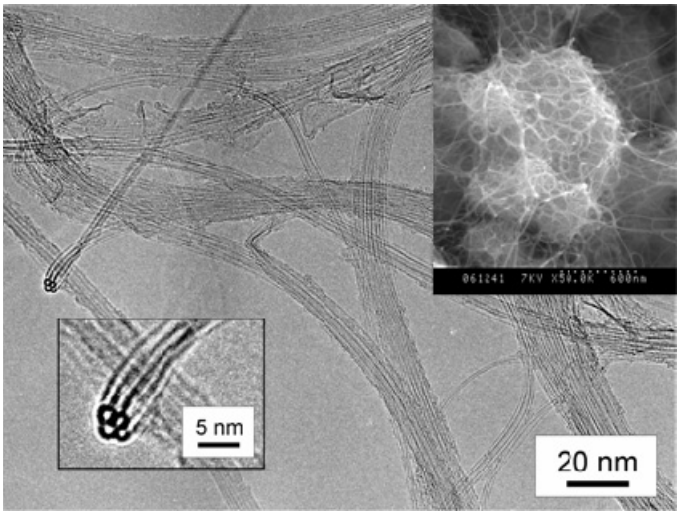

Figure 1. TEM image of high-purity SWNTs synthesized from alcohol. The insets show SWNTs grown on zeolite (upper) and a bundle cross-section (lower).

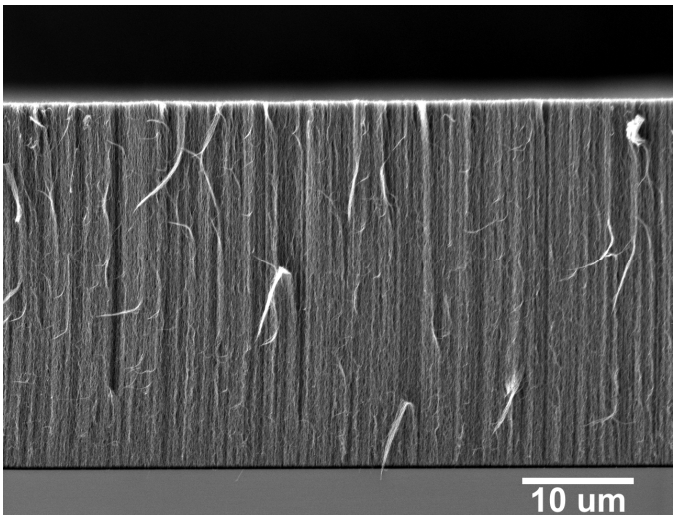

Figure 2. VA-SWNTs grown on a quartz substrate

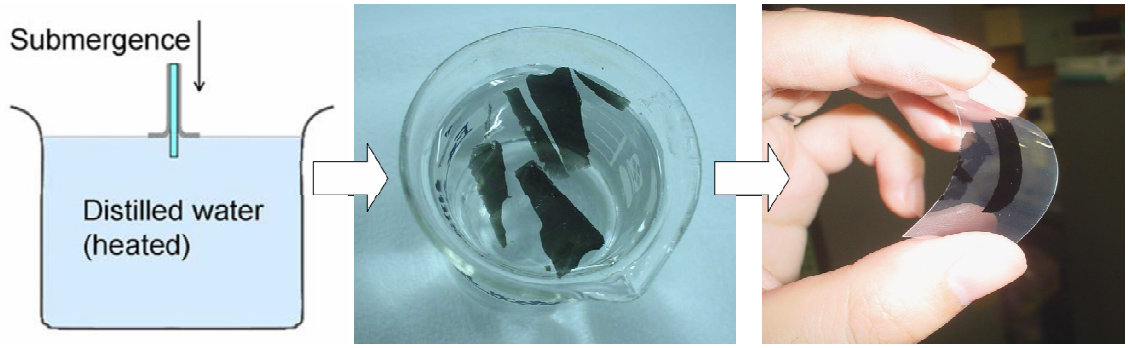

Figure 3. The hot-water assisted removal and transfer of VA-SWNT films.

minutes. VA-SWNT growth can occur at different flow rates and pressures, but typical values are 300-500 sccm at a pressure of 1-2 kPa. As shown in figure 2, VA-SWNT films produced by this method can exceed 30 μm in thickness.

ANISOTROPIC PROPERTIES

Due to the one-dimensional nature of SWNTs, many of their properties such as optical absorption, electrical and thermal conduction, and mechanical strength [25] are highly anisotropic. However, these properties are often difficult to measure experimentally because SWNTs tend to grow randomly when synthesized. The synthesis of VA-SWNTs provided a new opportunity to measure some of these interesting, anisotropic properties by providing samples of preferentially aligned SWNTs.

Anisotropic optical properties of our VA-SWNT films have been investigated by polarized optical absorption and resonance Raman spectroscopy [4, 26, 27]. Some of these studies were made considerably simpler by removing the VA-SWNT film from the quartz substrate on which it was synthesized, and transferring it onto a different substrate more conducive to handling and measurement. This was accomplished by a hot-water assisted method described in Ref. 28, and is shown in Figure 3. The significance of this method is that the SWNTs remain vertically aligned even after transfer. Many other measurements, as well as potential applications are expected to be simplified by using this approach. One application already realized by employing this transfer method is an all-fiber mode-locked laser, which was passively mode-locked by VA-SWNTs attached onto the optical fiber [29]. Combining this method with other micro-fabrication techniques, we have been pursuing experiments aimed at measuring the thermal conductivity of the aligned SWNTs, which is also expected to be highly anisotropic [24].

STATIONARY DIFFUSIVE-BALLISTIC HEAT CONDUCTION

Molecular dynamics simulations

The carbon-carbon interactions were modeled using Brenner potential [30] in a simplified form [31] where the total potential energy of the system is expressed as,

$$E_b = \sum_i \sum_{j(i<j)} \left[V_R(r_{ij}) - B^*_{ij} V_A(r_{ij}) \right] \quad (1)$$

Here, $V_R(r)$ and $V_A(r)$ are repulsive and attractive force terms, which take a Morse type form with a certain cut-off function. B^*_{ij} represents the effect of the bonding order parameters. As for the potential parameters, we employ the set that was shown to reproduce the force constant better (Table 2 in [30]). The velocity Verlet method was adopted to integrate the equation of motion with the time step of 0.5 fs.

The application of classical approach is encouraged by the expected dominant contribution on the heat conduction from phonons compared with that from electrons [32]. While the electric thermal conductance for semi-conducting SWNTs is expected to be negligible, contribution of electric thermal conductance in metallic SWNTs has been calculated to be minor (~10%) at room temperature [33].

The dispersion relations have been calculated for the current potential function [16, 17, 20]. The overall feature of dispersion relations obtained from MD simulations agrees with the reported theoretical models [1, 34], especially well with the mechanical model of Mahan and Jeon [34].

Thermal conductivity calculations

Thermal conductivity λ of an SWNT was measured with non-equilibrium MD simulations. After reaching an isothermal state at 300 K with the auxiliary velocity scaling control, the temperature controlled layers on both ends of the SWNT were activated to apply a temperature difference of 20 K. Eventually the temperature profile converges to a stationary state with quasi-linear gradient. The simulation time ranges within 3-18 ns as the data-convergence time depends on the system size and temperature control methods. By calculating the heat flux along the tube from the energy budgets of the thermostats, λ was calculated through the Fourier's law $q = -\lambda\, dT/dz$. The cross-sectional area A of a nanotube was defined using the ring of

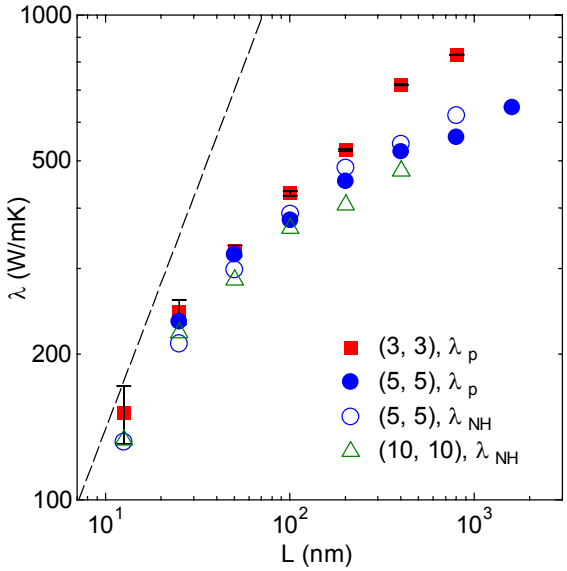

Figure 4. Length and diameter dependences of SWNT thermal conductivity. Subscripts P and NH indicate the values computed using the phantom technique and Nose-Hoover thermostats, respectively. Dashed line is $\lambda \propto L$ to indicate the slope in case of pure ballistic phonon transport. The fitting error bars are drawn only for the case of (3, 3) SWNTs, which exhibited the largest error among all the cases.

van der Waals thickness πbd, where b=0.34 nm is van der Waals thickness.

Length effect on SWNT thermal conductivity

In figure 4, thermal conductivity of (5, 5) SWNTs calculated using phantom technique (λ_P) [16, 17] and Nose Hoover thermostats (λ_{NH}) [35, 36] are marked with solid and open circles, respectively. Despite the differences in temperature control techniques, differences between λ_P and λ_{NH} were minor in the examined range of L, on observing the general trend of the length dependence of SWNT thermal conductivity. The overall trend of the slope ($\partial\lambda/\partial L$) clearly indicates the gradual transition from nearly pure ballistic to diffusive-ballistic phonon transport. When all the phonons experience ballistic phonon transport, λ is proportional to L (constant thermal conductance). The asymptotic match of the data to $\lambda \propto L$ (dashed line) suggests nearly pure ballistic phonon transport at the short SWNT limit. Note, on considering the significant phonon population in the wide range of phonon branches at room temperature, we expect contributions on the heat conduction not only from ballistic transport of acoustic phonon modes but also from that of various optical phonon modes in the small L regime. The gradient $\partial\lambda/\partial L$ gradually decreases as L increases since phonon mean free paths gradually become shorter relatively to L i.e. diffusive phonon transport is gradually enhanced with respect to ballistic phonon transport. The positive gradient at the upper bound indicates that the limit of the ballistic phonon transport exceeds a micrometer.

NON-STATIONARY DIFFUSIVE-BALLISTIC HEAT CONDUCTION

Simulation methods

A 25nm long (5,5)-SWNT was locally heated on 6 consecutive unit cells around the centre of the tube (z=0) with a heat pulse generated by connecting the region to the Nose-Hoover thermostat [35, 36] kept at 1000 K, for a time duration of 0.4 ps. Here, z denotes the axial direction. The system responds to the thermostat with the relaxation time of 4 fs. After disconnecting the thermostat, the total energy of the nanotube is kept at constant. As our intention is to apply and observe only the heat in the nanotube but not the stress (pressure) waves, both excitation and sampling were done in terms of the coherent molecular motions by canceling the total momentums of both the bulk and the heated region. The initial tube temperature is 50 K. The local instantaneous temperature for each unit-cell is defined through the instantaneous kinetic energy. The temperature profile was computed from ensembles of typically 40 simulations with different random initial condition. The computational cell was subjected to the periodic boundary condition, therefore the simulation models an infinitely long SWNT with local heat pulse applied at every L. The length L is 25 nm, long enough to acquire sufficient data before phonons collide through the periodic boundary.

Non-Fourier heat conduction

The isotherm contours shown in figure 5(a) depict the overall spatio-temporal history of the temperature. The picture shows how the heat supplied at the origin diffuses over half of the field (z>0). Figures 5 (b)-(d) show the isotherms for longitudinal, radial and circumferential components, respectively. The results of the simulations exhibit the heat wave of collective phonons traveling from the centered heated region of the SWNT towards the boundaries. In figure 5 (b-d), group velocities of LA (longitudinal acoustic), F (flexure) and TA (transverse acoustic) phonons under the Debye approximation (c_D) are denoted with solid lines. These long wavelength phonons travel without decaying until they reach the periodic boundary, which suggests that their ballistic length are equivalent to or larger than L/2. An interesting feature of the contour plot is the energy transported with slower group velocity than c_D visualized as streaks stretching from near the origin to both positive and negative z-directions (denoted with solid lines). The phonons forming the heat flux possess dominant energy among all the phonons, yet exhibit smaller group velocity than c_D. The decomposed isotherms [figure 5(b-d)] show that the observed heat wave is the superposition of heat waves of different directional components. As denoted with dashed lines, the collective phonons clearly exhibit the wavelike nature. Comparing the energy intensity of the heat

waves, the radial heat wave (H_R) contains approximately double the energy of the longitudinal heat wave (H_L) and the circumferential component plays a minor role. The propagation speeds of the heat waves are c_{HL} = 8 km/s and c_{HR} = 4 km/s.

Modal analyses of non-stationary phonon transport

The dispersion relations suggest that the Debye approximation may be too simple to describe the evolutions of broad phonon bands excited by the local heat pulse. On carrying out a modal analysis on such intermittent phenomena, the wavelet technique is useful as it allows us to follow the instantaneous spectrum altering in time. Furthermore, it can be tuned to adapt to the relaxation time that generally becomes small with increasing frequency. Here, the temporal wavelet transformation was performed on a time signal obtained from a single carbon atom using the Morlet wavelet,

$$\phi(\nu,t,\Delta t) = \exp(2\pi i \nu t)\exp\left[-\left(\frac{t}{\Delta t}\right)^2\right], \qquad (2)$$

as the mother wavelet, where Δt is the characteristic width of the wavelet. By repeatedly performing the transformation for all the carbon atoms, one can obtain temporal spectra of each velocity component for the entire spatio-temporal field.

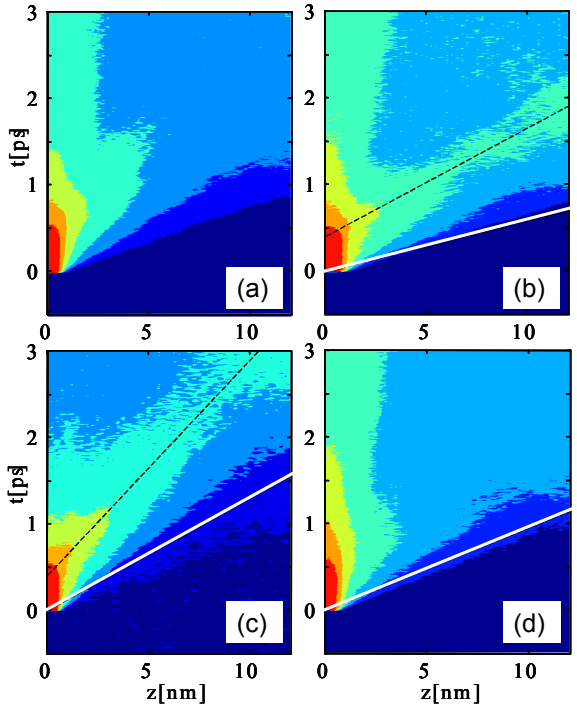

Figure 5. Spatio-temporal isotherms of (5,5)-SWNT subjected to a heat pulse at the origin. Figures denote the (a) overall temperature, (b) longitudinal, (c) radial and (d) circumferential components. White lines indicate c_D and dashed lines the propagation speed of heat waves.

Consequently, we define the spectral temperature as,

$$\theta_p(\nu,z,t) = \frac{1}{n}\sum_i^n \left[P(\nu,z,\phi_i,t) - P_0(\nu)\right]. \qquad (3)$$

The power spectrum P is ensemble averaged value of 10 numerical experiments and P_0 denotes the spectrum at equilibrium. The data are averaged over a unit cell with n molecules to project the spectrum to the 1D space.

In figure 6, the results are presented as temporal sequences of spectral contours in the (v,z)-field for radial components, respectively. The input heat pulse excites a wide range of frequency components. Note that since the nanotube is initially excited to a strongly non-equilibrium state, the phonon population is far off the statistical phonon distribution at equilibrium. Such state with high phonon populations in the high frequency optical branches can also be observed on subjecting a nanotube to optical excitations. The receptivity of an SWNT to the local excitation reflects the phonon density of state of the nanotube. As a consequence, in a broad range of frequency in radial components, there are energy fluxes that exhibit distinct propagation, which is best observed in the local spectral peaks detaching from the centre (z=0) and traveling toward the boundary. The trend is most evident in the distinct energy around 9 THz in the radial component, which corresponds to the band of large local density of states [16, 17].

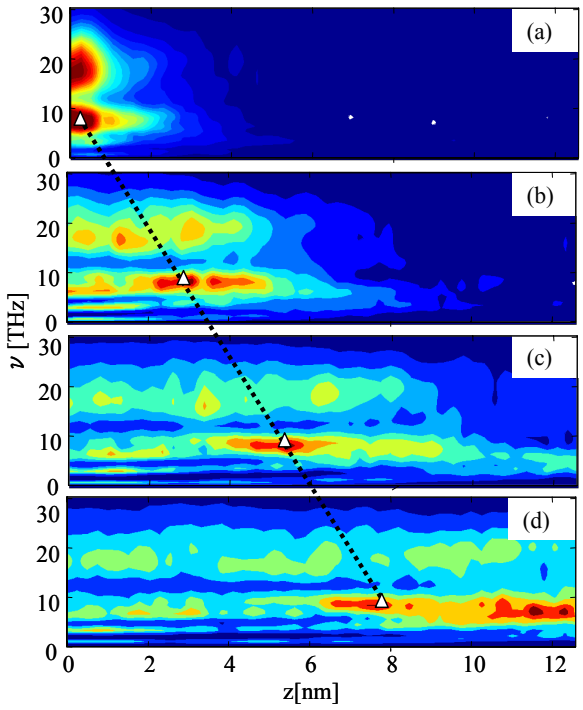

Figure 6. Temporal sequences of spectral temperature $\theta_p(v,z,t)$ of radial velocity component for (z>0). Figures denote spectra at (a) t=0.5, (b) 1.2, (c) 1.9 and (d) 2.7 ps.

The propagation speed of the band peak marked with triangles was confirmed to correspond with c_{HR}. As the observed energy transport consists of a range of frequency band beyond the upper limit of the branch of transverse acoustic-like flexure mode [34], significant energy of the present heat wave should reside in the transverse optical phonons. The results indicate the ballistic transport of a range of optical phonons. Although the relaxation time of those phonon modes are considerably shorter than those of low frequency modes including acoustic phonons, they can influence the heat conduction of relatively short nanotubes with length of nanometers.

HEAT TRANSFER OF SWNT IN PRACTICAL SITUATIONS

Isotope effects on SWNT thermal conductivity

Thermal conductivity of nanotube with randomly distributed ^{13}C with various ratios was calculated [24]. As seen in figure 7, the general trend of the results shows that the thermal conductivity decreases as the number ratio of ^{13}C increases due to the enhancement of phonon scattering. The results of the current MD simulations suggest that, at the room temperature, the isotope effect on the heat conduction of SWNTs is minor compared with that on the diamonds, where about 30 % thermal conductivity reduction was experimentally observed for mixing ratio of 1 %. Two cases with different length were simulated at 300 K in order to examine the size dependence of the isotope effect. As shown in figure 7, the variation of the thermal conductivity between the two results is almost constant. One could understand that the additional long wavelength phonons by lengthening the nanotube are not influenced by the isotopes whose effects are localized in relatively short atomic length scale. The temperature dependence was tested by lowering the temperature of the 50 nm nanotube to 100 K. Note that this case violates the limitation of the classical MD simulation, which cannot reproduce the correct heat capacity at low temperature. Still, this type of case studies should be beneficial to gain insights in terms of molecular dynamics. The analyses allow us to probe the influence of the isotope effect on phonon mean free path. If we assume the quantum effect on the heat capacity and isotope effect on the phonon mean free path to be independent of each other at low temperature, the proper thermal conductivity can be roughly estimated by multiplying thermal conductivity calculated by the MD simulations with the ratio of reduction in heat capacity due to the quantum effect. By lowering the temperature, the phonon mean free path becomes longer due to the reduction of thermal scattering. As seen in figure 7, the reduction ratio does not show major dependence on the temperature, hence the current simulation results do not suggest a significant influence of the phonon mean free path on the isotope effects.

SWNT isotope-superlattices

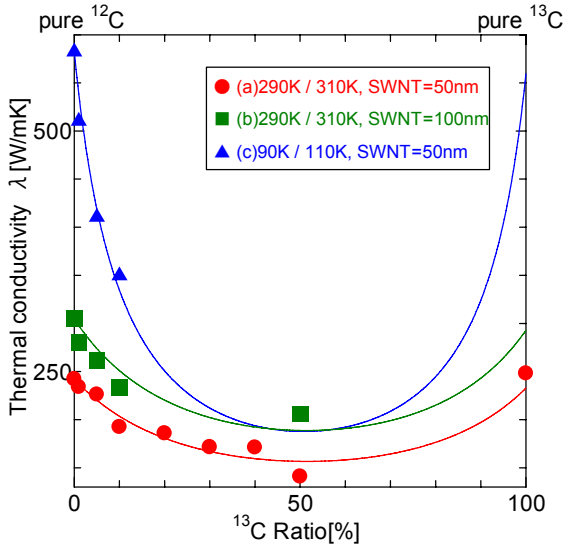

Figure 7. Effect of ^{13}C isotope on thermal conductivity of SWNT.

Simulations were done for armchair SWNTs with chirality index of (5,5). Superlattice structures were constructed by alternately connecting (5,5)-SWNTs with different mass [23]. Figure 8 denotes the isotope superlattice with cells of ^{12}C and ^{13}C with a certain period thickness Δz. Simulations were performed for various Δz and L. Before imposing the temperature gradient, the average temperature of the system was set at 300 K with the auxiliary velocity scaling control. Measurements were started when the quasi-stationary state was achieved by the phantom temperature control with temperature difference of 20 K. The data presented here are averaged over 10-20 ns. A typical time-averaged temperature profile exhibits fluctuation with well-defined length-scale corresponding to $\Delta z/2$ hence the effective temperature gradient was obtained by a linear least square fit. Heat fluxes passing through the nanotube remains constant as in the simulations for pure ^{12}C-SWNTs.

As shown in figure 9, the results of the simulations at the room temperature exhibit that λ takes a minimum value at Δz_{cr}~4 nm. The value is apparently much smaller than the conventional phonon mean free path of SWNTs. Although, the mean free path of the superlattice SWNTs may well be shorter than that of the pure ^{12}C-SWNT, it should be within the allowable variation estimated by the maximum reduction ratio, $(\lambda_0-\lambda)/\lambda_0$, where λ_0 is λ of pure ^{12}C-SWNTs. On considering the thermal conductivity in terms of the mean contribution from phonons i.e. Cvl, where C and v are representative heat capacity and group velocity, reduction ration of the mean free path l should not be more than $(\lambda_0-\lambda)/\lambda_0$,which is about 45 % at Δz_{cr}, even if we ignore the reduction of v due to the zone-folding effect.

Let us now think in terms of the contribution of each phonon to heat conduction, i.e. $\sum_i C_i v_i l_i$ in the regime with dominant influence of thermal boundary resistance (TBR)

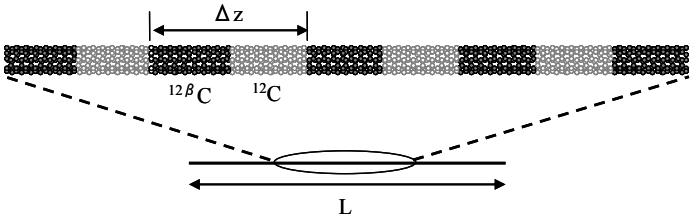

Figure 8. ^{12}C-^{13}C (5,5)-SWNT superlattice with period thickness Δz.

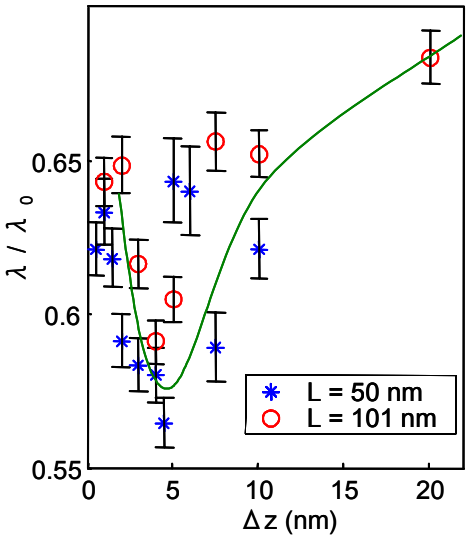

Figure 9. Dimension-less effective thermal conductivity of ^{12}C-^{13}C SWNT superlattice for a range of period thicknesses Δz, where λ for the pure ^{12}C-SWNT (λ_0) is 310 W/mK (L=50 nm) and 370 W/mK (L=101 nm).

($\Delta z > \Delta z_{cr}$). We assign the phonons into three categories with different contribution to λ. The first one is the fully ballistic phonons ($l_i \geq L$) which have Δz-invariant contribution to the conduction due to the phonon tunneling effect. The second one is the quasi-ballistic (diffusive-ballistic) phonons with $0<l_i<L$, whose contribution to λ is Δz dependent. The third one is the stationary phonons with negligible contribution to heat conduction due to small production of group velocity and free paths, $v_i l_i$. The phonons in the second category are the only ones with noticeable contribution to the dependence of λ on Δz in the TBR dominant regime. Therefore, if there is any mean free paths that should scale with Δz_{cr} that is the local mean free path of the diffusive-ballistic phonons.

Thermal conductance at an SWNT junction

One example of the interesting features of the system with nanotube junctions is the thermal conductance at the junction of nanotubes with different chiralities [24]. The simulated system is shown in figure 10. In this case a (12, 0) zigzag nanotube on the left-hand side and a (6, 6) armchair nanotube were smoothly connected using 5-membered and 7-membered rings at the junction. By applying different temperatures at each end, temperature distribution was measured as in figure 11. The temperature jump at the junction is clearly observed. This temperature jump can be modeled by assuming that there is a virtual boundary between two nanotubes with different structures. Now, we consider the thermal boundary conductance (TBC) of the virtual interface which relates the temperature drop and the heat flux through the boundary as,

$$K = \frac{Q}{A\Delta T}. \qquad (4)$$

TBC at the junction is calculated as 1.4×10^4 MW/m^{2}K. We have also tried various combinations of SWNTs whose diameter ratio ranges up to about 2.

CONCLUSIONS

Vertically aligned films of SWNTs were synthesized on quartz by the alcohol catalytic CVD method. These aligned films can be transferred from the substrates on which they are grown onto a new, arbitrary surface by a simple hot-water assisted technique. Using this technique conserves the vertically aligned morphology, and allows the VA-SWNTs to be adapted to various experimental constraints. This has helped to simplify the measurement of various anisotropic properties of SWNTs, as well as their inclusion in related applications.

Various heat transfer topics of SWNTs have been investigated using MD simulations. Stationary MD simulations were performed to investigate the SWNT heat conduction at room temperature in terms of phonon transport. The length effect of the SWNT thermal conductivity was identified, and the gradual transition from nearly pure ballistic phonon transport to diffusive-ballistic phonon transport was clearly observed. Diffusive-ballistic nature of the heat conduction in SWNT was also visualized by performing non-stationary MD simulations. Non-Fourier heat conduction was observed, where the heat was conducted in a wave-like form. Furthermore, attenuation of the heat conduction due to the isotope effect was quantified. The task of intrinsic thermal boundary resistance is further investigated by formulating a SWNT isotope superlattice and the effective thermal conductivity was found to take a minimum value at certain period thickness. Finally, thermal boundary conductance at the junction of nanotubes with different chiralities was computed.

ACKNOWLEDGMENTS

This work is supported by the Grants-in-Aid for Scientific Research #19206024.

REFERENCES

1. R. Saito, G. Dresselhaus and M. S. Dresselhaus, Physical Properties of Carbon Nanotubes, Imperial College Press, London (1998).

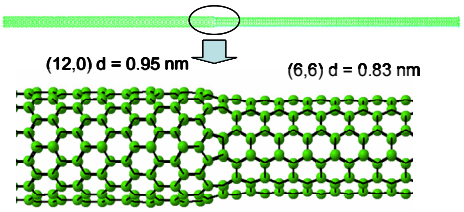

Figure 10. Junction of two different SWNTs.

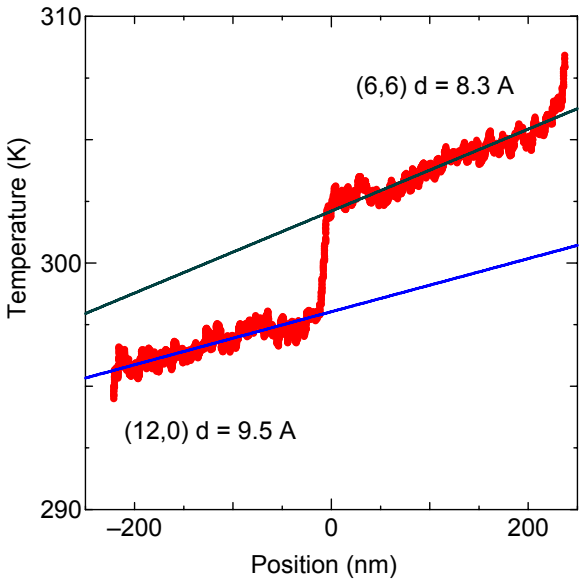

Figure 11. Temperature jump at the junction by local increase in the thermal resistance.

2. S. Maruyama, R. Kojima, Y. Miyauchi, S. Chiashi and M. Kohno, Chem. Phys. Lett., 360 (2002) 229.
3. Y. Murakami, S. Chiashi, Y. Miyauchi, M. Hu, M. Ogura, T. Okubo and S. Maruyama, Chem. Phys. Lett., 385 (2004) 298.
4. Y. Murakami, E. Einarsson, T. Edamura and S. Maruyama, Phys. Rev. Lett., 94 (2005) 087402.
5. S. Maruyama, E. Einarsson, Y. Murakami and T. Edamura, Chem. Phys. Lett., 403 (2005) 320.
6. K. Hata, D.N. Futaba, K. Mizuno, T. Namai, M. Yumura and S. Iijima, Science, 306 (2004) 1362.
7. G. Zhong, T. Iwasaki, K. Honda, Y. Furukawa, I. Ohdomari and H. Kawarada, Chem. Vap. Dep., 11 (2005) 127.
8. G. Zhang, D. Mann, L. Zhang, A. Javey, Y. Li, E. Yenilmez, Q. Wang, J.P. McVittie, Y. Nishi, J. Gibbons and H. Dai, Proc. Natl. Acad. Sci., 102 (2005) 16141.
9. G. Eres, A.A. Kinkhabwala, H. Cui, D.B. Geohegan, A.A. Puretzky and D.H. Lowndes, J. Phys. Chem. B, 109 (2005) 16684.
10. Y.-Q. Xu, E. Flor, M.J. Kim H. Behrang, H. Schmidt, R.E. Smalley and R.H. Hauge, J. Am. Chem. Soc., 128 (2006) 6560.
11. L. Zhang, Y. Tan, D.E. Resasco, Chem. Phys. Lett., 422 (2006) 198.
12. S. Noda, H. Sugime, T. Osawa, T. Yoshiko, S. Chiashi, Y. Murakami, S. Maruyama, Carbon, 44 (2006) 1414.
13. S. Berber, Y-K. Kwon and D. Tománek, Phys. Rev. Lett., 84 (2000) 4613.
14. C. Yu, L. Shi, Z. Yao, D. Li and A. Majumdar, Nano Lett., 5 (2006) 1842.
15. E. Pop, D. Mann, Q. Wang, K. Goodson and H. Dai, Nano Lett., 6 (2006) 96.
16. S. Maruyama, Physica B, 323 (2002) 193.
17. S. Maruyama, Micro. Therm. Eng., 7 (2003) 41.
18. R. Livi and S. Lepri, Nature, 421 (2003) 327.
19. N. Mingo and D. A. Broido, Nano Lett., 5 (2005) 1221.
20. J. Shiomi and S. Maruyama, Phys. Rev. B, 73 (2006) 205420.
21. D. D. Joseph, L. Preziosi, Rev. Mod. Phys., 62 (1990) 375.
22. S. Volz, J. B. Saulnier and M. Lallemand, Phys. Rev. B, 54 (1996) 340.
23. J. Shiomi and S. Maruyama, Phys. Rev. B, 74 (2006) 155401.
24. S. Maruyama, Y. Igarashi, Y. Taniguchi and J. Shiomi, J. Therm. Sci. Tech., 1 (2006) 138.
25. M.S. Dresselhaus, G. Dresselhaus and Ph. Avouris, Carbon Nanotubes: Synthesis, Structure, Properties, and Applications, Springer-Verlag, Berlin, 2001.
26. Y. Murakami, E. Einarsson, T. Edamura and S. Maruyama, Carbon, 43 (2005) 2664.
27. Y. Murakami, S. Chiashi, E. Einarsson and S. Maruyama, Phys. Rev. B, 71 (2005) 085403.
28. Y. Murakami and S. Maruyama, Chem. Phys. Lett., 422 (2006) 575.
29. Y.-W. Song, E. Einarsson, S. Yamashita and S. Maruyama, Opt. Lett., 32 (2007) 1399.
30. D. W Brenner, Phys. Rev. B, 42 (1990) 9458.
31. Y. Yamaguchi and S. Maruyama, Chem. Phys. Lett., 286 (1998) 336.
32. J. Hone, M. Whitney, C. Piskoti and A. Zettl, Phys. Rev. B., 59 (1999) R2514.
33. T. Yamamoto, S. Watanabe and K. Watanabe, Phys. Rev. Lett., 92 (2004) 075502.
34. G. D. Mahan and G. S. Jeon, Phys. Rev. B, 70 (2004) 075405.
35. S. Nose, J. Chem. Phys., 81 (1) (1984) 511.
36. W. G. Hoover, Phys. Rev. A, 31 (1985) 1695.